Phase diagram of the Cairo pentagonal XXZ spin-$\frac{1}{2}$ magnet under a magnetic field

Arnaud Ralko
Institut Néel, UPR2940, CNRS et Université de Grenoble, Grenoble, F-38042 France
(Received 25 July 2011; revised manuscript received 10 September 2011; published 28 November 2011)

The phase diagram of the XXZ spin-1/2 magnet, equivalent to hard-core bosons, under a staggered magnetic field and on the Cairo pentagonal lattice is computed at zero and finite temperature by using a cluster mean-field theory and a stochastic series expansion quantum Monte Carlo. The complex connectivity and the frustration lead to unconventional phases such as a 1/3 ferrimagnetic plateau stabilized by quantum fluctuations as well as a 5/12 topological phase induced by a local ice-rule constraint. We also report the presence of a ferrimagnetic superfluid and its thermal melting. Finally, we discuss the ferro- and antiferro- magnetic (hopping sign) cases.

DOI: 10.1103/PhysRevB.84.184434 PACS number(s): 75.10.Jm, 05.30.−d, 05.50.+q

I. INTRODUCTION

In recent years, important discoveries in strongly correlated physics have been reported in systems where frustration plays a central role. Geometrical frustration is very interesting in that respect. A large variety of unusual phases is encountered, from (insulating) exotic spin liquids[1–3] to superconductivity.[4] Recent developments in frustrated *optical lattices* of cold atoms open new directions for stabilizing exotic bosonic phases such as supersolids[5] and Bose metals.[6–8]

A case of interest is that of *ice-rule* systems, for which highly degenerate classical ground state are governed by a local constraint.[9] For spin 1/2 (boson), it corresponds to a fixed number of up (occupied) and down (empty) spins (sites) on each elementary brick: a tetrahedron on pyrochlore and checkerboard lattices[10,11] or a triangle on the kagome.[12] They provide striking features such as charge fractionalization,[13] Coulomb-gas phases, and even *magnetic monopoles.*[14] Their quantum melting is of broad interest but remains a highly nontrivial question; aside from the strength of the interactions, the lattice geometry can play a relevant role. Some works in this direction revealed exotic phases, e.g., a commensurate *resonating valence bond* supersolid on the checkerboard lattice.[15] Hence, it is natural to search for ice-rule systems with more complex geometries such as inequivalent site lattices.[16]

Recently, Ressouche *et al.* rendered the two-dimensional Cairo pentagonal structure accessible to experiments by proposing the iron-based compound $Bi_2Fe_4O_9$.[17] So far it is the only known compound with this geometry: a spin-5/2 antiferromagnet made of identical nonregular pentagons with a site-dependent connectivity c_i of three (z_3 site) and four (z_4 site) neighbors as depicted in Fig. 1(a). Note that this Cairo lattice is the dual of the Shastry-Sutherland lattice for which the ground state can be a spin liquid.[19] From the quantum side, substituting iron atoms with copper ones in $Bi_2Fe_4O_9$,[18] or creating complex optical lattices, the square-based Cairo lattice, for example [Fig. 1(b)], is undoubtedly a major challenge. However, in view of the recent original phases reported in frustrated systems,[20–22] inequivalent-site structures possess all the ingredients that cause one to expect unconventional physics.

In this paper, we study a spin-1/2 magnet under a staggered magnetic field, or, equivalently, the extended hard-core boson Hubbard model, on the Cairo pentagonal lattice. We report a rich phase diagram obtained both at zero and at low temperature. We focus on the different insulating phases: a *topological* ice rule of two bosons per pentagon, a 2/3 checkerboard, and a pure quantum 1/3 *ferrimagnetic* phase with no local constraint. Moreover, a large region of ferrimagnetic superfluid is identified as well as its Kosterlitz-Thouless (KT) transition[23] at strong repulsion induced by thermal fluctuations. We also compare the ferro- and antiferromagnetic cases (sign of hopping) and discuss the case of a uniform magnetic field (nature of the chemical potential).

II. MODEL AND METHODS

Spin 1/2 on the pentagonal lattice can be described by an extended hard-core boson Hubbard model, with a repulsive nearest-neighbor interaction V, a hopping t, and a chemical potential μ_i, given by

$$\mathcal{H} = -t\sum_{\langle i,j\rangle}(b_i^\dagger b_j + \text{h.c.}) + V\sum_{\langle i,j\rangle} n_i n_j - \sum_i \mu_i n_i, \qquad (1)$$

where i is the site index, $b_i^\dagger$ is the creation operator, and n_i the number of bosons. The correspondence is done by mapping $S_i^\dagger = b_i^\dagger$ and $S_i^z = n_i - 1/2$ and Eq. (1) is equivalent to a XXZ spin-1/2 magnet with spin couplings $J_z = V$ and $J_\perp = -2t$,

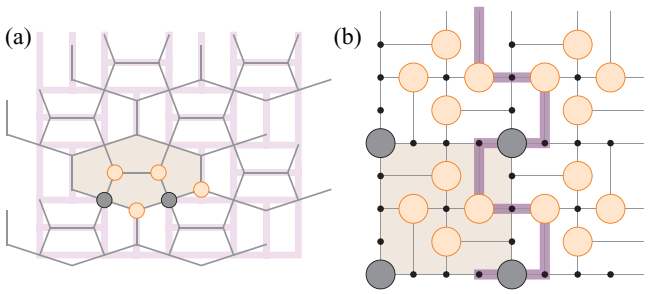

FIG. 1. (Color online) (a) The Cairo pentagonal lattice and its six-site unit cell (shaded hexagon) containing two z_4 sites (dark circles) and four z_3 sites (light circles). The continuously deformed square-based *Cairo* lattice used in this work is displayed in the background. (b) One of the authorized 5/12 topological ice-rule configurations with two spins up (bosons) per pentagon (large circles). Thick line: typical winding loop along which a shift of all encountered bosons at one lattice site preserves the ice-rule constraint. Shaded square: the 12-site cluster (2 unit cells) used in the CMFT.

under an effective magnetic field h_i. The chemical potential μ_i is an adjustable parameter.[20] This leads to two important cases for systems with anisotropic c_i; it can be either (a) site dependent or (b) constant. In case a, if μ_i is set to $\mu + c_i V/2$, we have the well-known spin-1/2 magnet under a uniform magnetic field.[24] In case b, the system experiences a staggered magnetic field $h_i = \mu - c_i V/2$ depending explicitly on the connectivity. Experimentally, this can occur in systems with alternating crystal structure and the possible presence of a Dzyaloshinskii-Moriya interaction.[25] These two cases are of great importance in quantum magnetism, but the latter case can obviously provide unexpected behaviors as has recently been shown in one-dimensional materials.[26] In the present work, we hence focus on the constant μ and draw out the rich phase diagram induced by the complex connectivity c_i. We use equivalently bosonic or spin language when appropriate.

To simplify the analysis, we map the parameters on a sphere described by two angles θ and ϕ in such a way that $\bar{\mu} = \sin\phi$, $\bar{t} = \cos\theta\cos\phi$, and $\bar{V} = \sin\theta\cos\phi$, where $(\bar{t},\bar{V},\bar{\mu})$ are dimensionless. We also consider a deformed square-based version of the original lattice [see Fig. 1(b)].

The phase diagram (Fig. 3) is obtained by using two numerical methods, the cluster mean-field theory (CMFT)[27] and a stochastic series expansion (SSE) quantum Monte Carlo (QMC),[28] at zero and finite temperature, respectively. The basis of the CMFT is to consider a finite cluster for which the internal bonds in Eq. (1) are treated exactly, whereas the boundary conditions are coupled to an external bath. Here we use the 12-site cluster shown in Fig. 1(b) (shaded region) and corresponding to two unit cells. The system is diagonalized and solved self-consistently. Note that for the triangular lattice, this method gives an excellent agreement with the QMC results.[29] Here it also allows us to consider the frustrated $t < 0$ case (antiferromagnet) in addition to the $T = 0$ properties. The SSE algorithm provides unbiased quantum simulations for very large system sizes, in our case, $N = l\sqrt{3/4} \times l\sqrt{3/4}$, with l up to 72 (3888 sites), and at finite temperature T. Usually, $T^{-1} = 2l$ is enough to focus on ground state properties.[30,31] At very large repulsion, however, the KT temperature T_{KT} drops significantly, and a finite temperature transition at low T is expected. In this work, the phase diagram is computed at $T^{-1} = 100 > 2l$ (up to $l = 48$) and thermal effects are considered.

We consider four quantities: x, the average number of bosons (spin magnetization); ρ_S, the superfluid density (spin stiffness) implemented via the winding numbers in the SSE;[28] p_n, the average number of pentagons with exactly n up-spins and the order parameter $M^2(\mathbf{q}) = \langle\psi_0|n(-\mathbf{q})n(\mathbf{q})|\psi_0\rangle/N$, with $n(\mathbf{q}) = \sum_i e^{i\mathbf{q}\cdot\mathbf{r}_i} n_i$ performed separately on all sites of the non-Bravais square-based lattice at $\mathbf{q} = (\pi,\pi)$ (M_{all}) and on the z_i sublattice at $\mathbf{q} = (0,0)$ (M_{z_i}).[31,32] As the square-based Cairo lattice is a depleted square lattice with extra bonds [longer bonds in Fig. 1(b)], a finite $M(\mathbf{q})$ is expected even for a disordered phase, as entirely explained in Ref. 31.

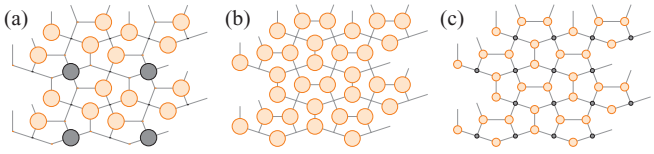

FIG. 2. (Color online) Schematic representation of the insulating phases in Fig. 3. Dark (light) circles represent z_4 (z_3) sites and their size is proportional to the magnetization (boson density). (a) A typical 5/12 topological ice-rule configuration, (b) the 2/3 checkerboard configuration, and (c) the quantum 1/3 ferrimagnetic configuration.

III. OVERVIEW OF THE PHASE DIAGRAM

Figure 3 depicts the zero (CMFT; dashed lines) and finite (SSE; symbols) temperature phase diagrams in the large repulsion limit $\theta/\pi > 0.3$, where insulating phases appear. To characterize the different phases, we have considered the two cut lines at fixed θ and ϕ, respectively, shown in Fig. 3. Since the phase diagram is very rich, we briefly introduce it in this paragraph before giving more details in the rest of the paper. Close to $\theta = \pi/2$ ($V/t \to \infty$), only reachable by the mean field, the frustration leads to two magnetization plateaux, at $x = 2/3$ and 5/12 (see Fig. 2), at $T = 0$. Surprisingly, when quantum fluctuations are turned on ($\theta < \pi/2$), a third insulating plateau arises, at $x = 1/3$. This insulator is not stabilized at the classical limit and is fully driven by quantum fluctuations and stabilized by the frustration ($t < 0$). The quantum melting of these lobes leads, in spin language, to a superfluid corresponding to different magnetizations (boson density) on each sublattice. Uncompensated phases have already been reported in systems with complex coordination.[16]

The finite T phase diagram is computed via the SSE method up to $\theta/\pi = 0.485$ (circles in Fig. 3). Stronger interaction results (shaded regions) are extrapolated. The main difference from the $T = 0$ case is the presence of disordered regions (Dis.) due to thermal fluctuations, the KT transition of the superfluid phases, and/or the melting of the insulating lobes. Note that small discrepancies between the methods cannot be avoided. In the following, we detail the phases in Fig. 3. In particular, we describe the ferrimagnetic character of the

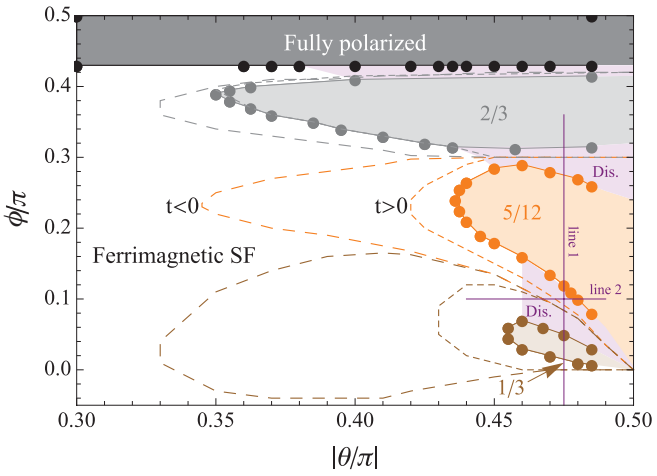

FIG. 3. (Color online) Phase diagram in the (θ,ϕ) plane and the comparison between zero (CMFT; dashed lines) and finite (SSE for $\theta/\pi < 0.485$; symbols) temperature. Insulating phases (lobes) are enhanced at zero temperature and by frustration ($t < 0$). The ferrimagnetic superfluid (SF) has a Kosterlitz-Thouless (KT) transition to a disordered region (Dis.) at finite T. Lines 1 and 2 are the scans used in Figs. 4 and 5, respectively.

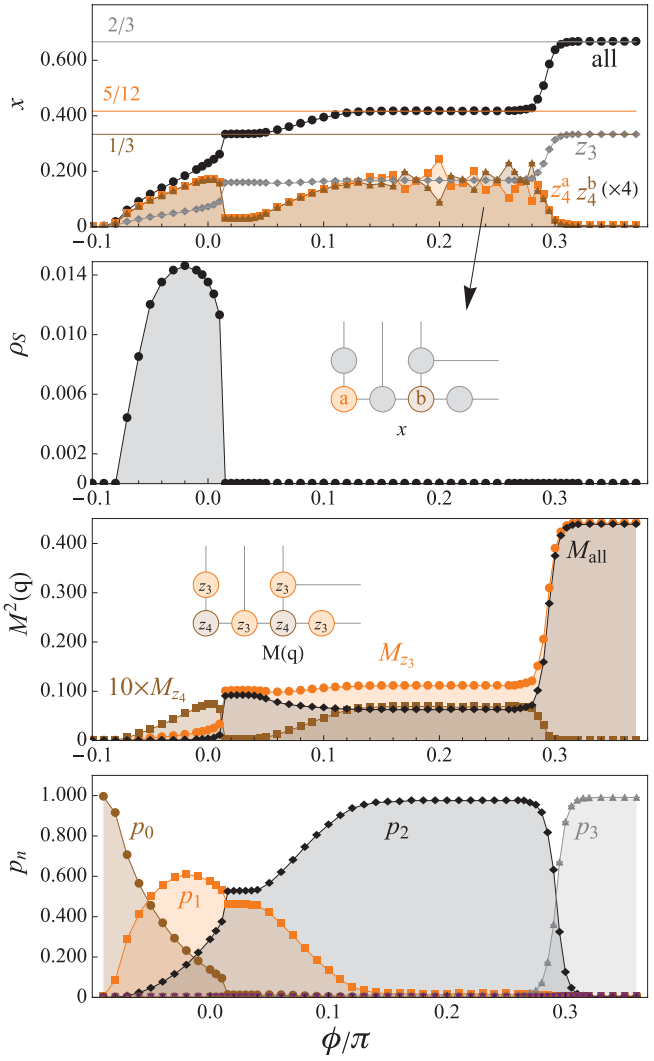

FIG. 4. (Color online) Scan along line 1 in Fig. 3 at strong repulsion ($\theta = 0.475\pi$), for the cluster size $l = 40$ and at finite T. From top to bottom: magnetization x (boson density), spin stiffness ρ_S (superfluid density), order parameter $M^2(q)$ at (π,π) for $M_{\rm all}$ (all sites) and (0,0) for M_{z_i} (z_i sublattice), and average number of pentagons p_n with n up-spins (bosons). Inset: Sublattices used for x and $M^2(q)$ indicated by arrows.

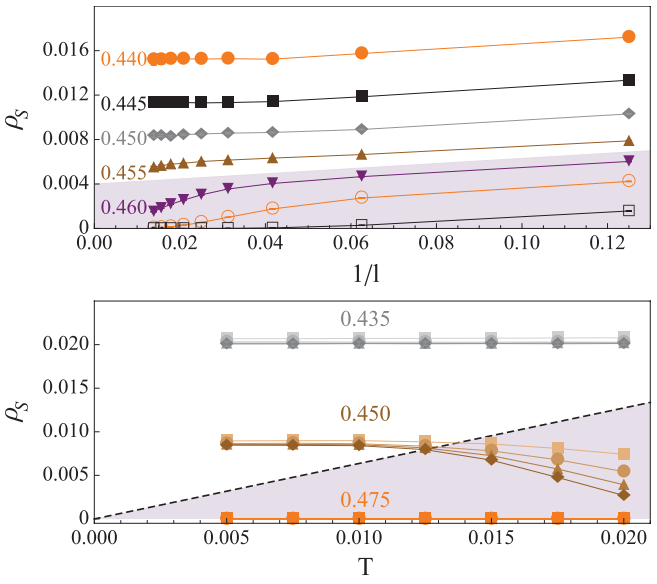

FIG. 5. (Color online) Scan along line 2 in Fig. 3 at $\phi/\pi = 0.1$ of ρ_S as a function of the size l at $T = 0.01$ (top) and as a function of T for sizes up to $l = 16$, 24, 32, and 40 (bottom; symbols). The dashed line is the $2T/\pi$ line, for which a crossing with $\rho_S(T)$ indicates the Kosterlitz-Thouless transition. Shaded areas: disordered phases in Fig. 3.

superfluid phase and provide a temperature analysis at strong interaction before presenting the unconventional insulators.

IV. SUPERFLUIDITY AND THERMAL FLUCTUATIONS

As mentioned above, at zero T and for θ small enough, the system is a superfluid ($\rho_S \neq 0$) with an on-site magnetization (boson density) depending on the connectivity c_i. We refer to this phase as the ferrimagnetic superfluid.[24] We have computed the four physical quantities following the two cut lines depicted in Fig. 3 at both fixed θ (line 1; Fig. 4) and fixed ϕ (line 2; Fig. 5). Figure 4 displays (from top to bottom) x, ρ_S, $M(q)$, and p_n, as a function of ϕ and at finite T.

More information can be obtained by computing x and $M(q)$ on sublattices z_3 and z_4 as well. For $\phi < 0.2\pi$, $x_{z_3} \neq x_{z_4}$, while $\rho_S \neq 0$, hence corroborating the presence of the superfluid. At $T = 0$ and for θ large enough ($>0.45\pi$), transitions either of first order between two lobes or of second order with a superfluid are observed (reinforced at $t < 0$). At finite T (SSE), disordered regions (Dis. in Fig. 3) with a finite compressibility $dx/d\phi \neq 0$ and $\rho_S = 0$ emerge, related to a KT transition; a finite ρ_S [broken U(1) symmetry] in two dimensions is indeed allowed up to a $T_{\rm KT}$ temperature. Figure 5 depicts the size scaling up to $l = 72$ (top) and the T dependence (bottom) of ρ_S for $\phi = 0.1\pi$ (line 2).

As shown in the upper panel in Fig. 5, a transition between $\rho = 0$ and $\neq 0$ occurs at the thermodynamic limit. For 2D systems, the KT transition is located by the universal jump at $\rho_S(T_{\rm KT}) = 2T_{\rm KT}/\pi$ plus some logarithmic finite-size corrections.[30] This is calculated in Fig. 5 for three representative values of θ/π along line 2: (i) deep in the superfluid phase (0.435), (ii) close to the transition (0.45), and (iii) in the $\rho_S = 0$ region (0.475). We obtain (i) $T < T_{\rm KT}$, (ii) $T_{\rm KT} \simeq 0.0125$ close to T, and (iii) $T_{\rm KT} \ll T$ with a KT transition at $\theta/\pi \simeq 0.46$. The finiteness of $T_{\rm KT}$ is nontrivial and beyond the scope of this paper. However, it is related to the propagation of defects during doping of an insulator. For example, adding a boson in the 5/12 ice-rule phase results in creating two p_3 defects with zero-energy dynamics. This would be compatible with a small but finite $T_{\rm KT}$ at the thermodynamic limit.

V. INCOMPRESSIBLE PHASES

A. The 2/3 checkerboard phase

In Fig. 4, at $\phi/\pi > 0.3$, all the pentagons carry three bosons ($p_3 = 1$), $\rho_S = 0$, and $M(q)$ is finite for the z_3 sublattice but 0 at the z_4 sites. This is in agreement with filled x_{z_4} sites and empty x_{z_3} sites. This order is a simple checkerboard crystal [Fig. 2(b)] and is the largest lobe in Fig. 3, with $\theta_{\rm max} \simeq 0.35\pi$

at $\phi \simeq 0.39\pi$ since adding one particle costs the energy $4V$. All z_3 sites are up-spins.

B. The 1/3 ferrimagnetic phase

The 1/3 plateau is one of the unexpected phases obtained in this geometry, which arises only under quantum fluctuations (see Fig. 3), at both 0 and finite T. It is stabilized under either a staggered or a constant[24] magnetic field, and its expansion is 10 times larger (in units of V/t) for $t < 0$. It is insulating ($\rho_s = 0$) with no ice-rule constraint ($p_{1,2} \neq 0$; Fig. 4) and no broken lattice symmetry.[32] The internal unit cell densities x_{z_3} and x_{z_4} mismatch (Fig. 4), showing a ferrimagnetic character at magnetization 1/3 [Fig. 2(c)]. As displayed in Fig. 4, at finite T the 1/3 phase is surrounded by two phase transitions, a first order with the superfluid phase for $\phi/\pi \simeq 0.01$ and a continuous transition with the disordered phase. At $T = 0$, however, the disordered phase is not present and a first-order transition between the 1/3 phase and the 5/12 one is obtained (dashed lines in Fig. 3). The tip of the 1/3 lobe in Fig. 3 is located at $\theta/\pi \simeq 0.455$, precisely where the first-order transition vanishes.

C. The topological ice-rule phase

The 5/12 plateau is stabilized when the magnetic field is staggered (constant μ_i). Stable at the Ising limit (CMFT), this phase is robust against both quantum and thermal fluctuations, specifically at $t < 0$ (Fig. 3). In Fig. 4, $\rho_S = 0$ and an average of 2 bosons at z_3 sites, compared to 0.5 at z_4 sites, per unit cell is observed. $M(q)$ is larger than the depletion-induced internal structure signal, indicating a clear difference between the sublattices.[31,32] With $p_2 = 1$, we deduce the presence of an ice rule of two bosons per pentagon. A typical configuration of this 5/12 phase is shown in Fig. 2(a). By labeling the z_4 sites inside a unit cell as z_4^a and z_4^b (inset in Fig. 4), we identify a finite distribution of $x_{z_4^a}$ and $x_{z_4^b}$ with respect to ϕ related to the degeneracy of the ground state. Classical zero-energy configurations in standard ice-rule systems can generally be connected by quantum tunneling of a finite number of particles on a closed path. This leads, through perturbation theory, to a quantum effective Hamiltonian, e.g., quantum dimer models[15,33,34] or loop models.[13,35] Here no such local moves are available; only winding loops invoking the boundary conditions instead [see Fig. 1(b)]. Bosons on such a loop have only two possible positions that respect the ice-rule constraint, and a tunneling from one to the other results in a new 5/12 configuration. For a cluster of size l, there are $l/4$ distinct contours in each direction (x and y). For a given configuration, the number of bosons on such a contour is a conserved quantity and each set of these quantities defines a topological sector. Only the global shift of the bosons along a winding loop can change this number and, thus, the topological sector; the system is protected from local disorder. Starting from the most symmetrical 5/12 configuration [Fig. 1(b)], the total number of winding loops is $l/2$. A shift of the bosons along one direction cancels the possible winding loops along the other. The number of connected configurations is then simply $\Omega = 2 \times 2^{l/4}$. The zero-temperature entropy per site hence scales as $\mathcal{S}/N = \frac{(l+4)\log 2}{3l^2}$ and vanishes at the $l \to \infty$ limit. Since all the configurations are frozen, the phase transition is not smooth, as confirmed by the sudden appearance of the distribution. We estimate the width of the 5/12 plateau by the expansion of this distribution, e.g., $0.13(1) \leqslant \phi/\pi \leqslant 0.26(1)$ in Fig. 4. To our knowledge, isolated sectors have always been reported in systems where local moves were also available.[33]

VI. CONCLUDING REMARKS

We report the phase diagram of spin-1/2 magnets (hard-core bosons) on the Cairo pentagonal lattice, at zero (CMFT) and finite (SSE) temperature. The anisotropic connectivity leads, at constant μ_i, to a staggered magnetic field.[25,26] Various insulating phases are identified, among which is a pure quantum-induced 1/3 ferrimagnetic phase, not stabilized in the Ising limit ($\theta = \pi/2$).[24] An original 5/12 topological ice-rule phase is evidenced, emphasizing the main difference between spin-1/2 systems under staggered and those under uniform fields. In this system, the effect of frustration ($t < 0$) enhances the insulating phases. Finally, a zero vs. finite T comparison reveals a KT transition located at strong repulsion as well as a partial melting of the lobes. The two methods employed here are in good agreement. Open issues remain, such as the complete description of the phase transitions and the temperature properties. Nevertheless, the spin-1/2 Cairo magnet is a very promising candidate for exploration of new states of matter.

ACKNOWLEDGMENTS

I thank O. Cépas and V. Simonet for discussions. I am indebted to A. Laüchli and D. Poilblanc for valuable critical comments on the manuscript. I am also grateful to N. Dempsey for careful rereading of the manuscript.

[1] P. Mendels, F. Bert, M. A. de Vries, A. Olariu, A. Harrison, F. Duc, J. C. Trombe, J. Lord, A. Amato, and C. Baines, Phys. Rev. Lett. **98**, 077204 (2007).

[2] F. Mila, F. Vernay, A. Ralko, F. Becca, P. Fazekas, and K. Penc, J. Phys. Condens. Matter **19**, 145201 (2007); A. Ralko, M. Ferrero, F. Becca, D. Ivanov, and F. Mila, Phys. Rev. B **76**, 140404(R) (2007).

[3] Y. Ran, M. Hermele, P. A. Lee, and X.-G. Wen, Phys. Rev. Lett. **98**, 117205 (2007).

[4] D. C. Johnston, J. Low Temp. Phys. **25**, 145 (1976).

[5] J. Ruostekoski, Phys. Rev. Lett. **103**, 080406 (2009).

[6] M. V. Feigelman, V. B. Geshkenbein, L. B. Ioffe, and A. I. Larkin, Phys. Rev. B **48**, 16641 (1993).

[7] D. Das and S. Doniach, Phys. Rev. B **60**, 1261 (1999).

[8] A. Paramekanti, L. Balents, and M. P. A. Fisher, Phys. Rev. B **66**, 054526 (2002).

[9] Ice rules bring novel features with respect to the bandwidth-controlled Mott transition at half-filling ($n = 1$), e.g., T. Yoshioka, A. Koga, and N. Kawakami, J. Phys. Soc. Jpn. **77**, 104702 (2008).

[10]M. J. Harris, S. T. Bramwell, D. F. McMorrow, T. Zeiske, and K. W. Godfrey, Phys. Rev. Lett. **79**, 2554 (1997).
[11]H. Ueda, H. A. Katori, H. Mitamura, T. Goto, and H. Takagi, Phys. Rev. Lett. **94**, 047202 (2005); D. L. Bergman, R. Shindou, G. A. Fiete, and L. Balents, *ibid.* **96**, 097207 (2006).
[12]A. S. Wills, R. Ballou, and C. Lacroix, Phys. Rev. B **66**, 144407 (2002).
[13]P. Fulde, K. Penc, and N. Shannon, Ann. Phys. **11**, 892 (2002); F. Pollmann, P. Fulde, and E. Runge, Phys. Rev. B **73**, 125121 (2006).
[14]For a review, see chapters by M. J. P. Gingras, R. Moessner, and K. S. Raman, in *Highly Frustrated Magnetism*, edited by C. Lacroix, P. Mendels, and F. Mila (Springer-Verlag, Berlin, 2010).
[15]A. Ralko, F. Trousselet, and D. Poilblanc, Phys. Rev. Lett. **104**, 127203 (2010).
[16]A. Jagannathan, R. Moessner, and S. Wessel, Phys. Rev. B **74**, 184410 (2006).
[17]E. Ressouche, V. Simonet, B. Canals, M. Gospodinov, and V. Skumryev, Phys. Rev. Lett. **103**, 267204 (2009).
[18]V. Simonet (private communication).
[19]K. S. Raman, R. Moessner, and S. L. Sondhi, Phys. Rev. B **72**, 064413 (2005).
[20]V. W. Scarola, E. Demler, and S. Das Sarma, Phys. Rev. A **73**, 051601(R) (2006).
[21]I. Titvinidze, M. Snoek, and W. Hofstetter, Phys. Rev. Lett. **100**, 100401 (2008).
[22]F. Hébert, G. G. Batrouni, X. Roy, and V. G. Rousseau, Phys. Rev. B **78**, 184505 (2008).
[23]J. M. Kosterlitz and D. J. Thouless, J. Phys. C **6**, 1181 (1973); J. M. Kosterlitz, *ibid.* **7**, 1046 (1974).
[24]A Cairo spin-1/2 Heisenberg model is currently being studied by I. Rousochatzakis, A. Laüchli, and R. Moessner (private communication, 2011); a similar 1/3 ferrimagnetic phase is discussed.
[25]M. Oshikawa and I. Affleck, Phys. Rev. Lett. **79**, 2883 (1997).
[26]J. Lou, C. Chen, J. Zhao, X. Wang, T. Xiang, Z. Su, and L. Yu, Phys. Rev. Lett. **94**, 217207 (2005); B. Xi, S. Hu, J. Zhao, G. Su, B. Normand, and X. Wang, e-print arxiv:1106.4605 (2011).
[27]E. Zhao and A. Paramekanti, Phys. Rev. B **76**, 195101 (2007).
[28]A. W. Sandvik, Phys. Rev. B **59**, R14157 (1999).
[29]S. R. Hassan, L. de Medici, and A.-M. S. Tremblay, Phys. Rev. B **76**, 144420 (2007).
[30]H. Kuroyanagi, M. Tsikamoto, and M. Tsubota, J. Phys. Soc. Jpn. **80**, 034603 (2011); N. Laflorencie and F. Mila, Phys. Rev. Lett. **99**, 027202 (2007).
[31]K.-K. Ng, Phys. Rev. B **81**, 094426 (2010).
[32]No Bragg peak is observed in the structure factor on the Bravais lattice (six-site unit cell).
[33]D. S. Rokhsarand, S. A. Kivelson, Phys. Rev. Lett. **61**, 2376 (1988).
[34]A. Ralko, M. Mambrini, and D. Poilblanc, Phys. Rev. B **80**, 184427 (2009).
[35]O. F. Syljuåsen and S. Chakravarty, Phys. Rev. Lett. **96**, 147004 (2006); O. Cépas and A. Ralko, Phys. Rev. B **84**, 020413(R) (2011).